CHEMBIOCHEM

DOI: 10.1002/cbic.200500061

A Fragment-Based Approach to Understanding Inhibition of 1-Deoxy-D-Xylulose-5-Phosphate Reductoisomerase

Ludovic Mercklé,[a] Ana de Andrés-Gómez,[a] Bethany Dick,[a] Russell J. Cox,*[a] and Christopher R. A. Godfrey[b]

The inhibition of 1-deoxy-D-xylulose-5-phosphate reductoisomerase (DXR) by fosmidomycin was studied by using a kinetic assay based on the consumption of NADPH and synthetic substrate. Fosmidomycin is a slow tight-binding inhibitor of DXR that shows strong negative cooperativity ($|h| = 0.3$) in binding. Cooperativity is displayed during the initial (weak, $K_{0.5} = 10\ \mu M$) binding event and does not change as the binding tightens to the equilibrium value of 0.9 nM over a period of seconds to minutes. A series of fosmidomycin fragments was examined, but all showed much weaker inhibition, in the mM range. A series of cyclic fosmidomycin analogues was also synthesised and tested, but these showed high-μM binding at best. None of the synthetic compounds showed time-dependent inhibition. We concluded that the slow tight-binding behaviour, and perhaps also cooperativity, are mediated by significant reorganisation of the active site upon fosmidomycin binding. This makes the rational design of new inhibitors of DXR difficult at best.

Introduction

The enzyme 1-deoxy-D-xylulose-5-phosphate reductoisomerase (DXR, EC 1.1.1.267) catalyses the interconversion of 1-deoxy-D-xylulose-5-phosphate (DXP; **1**) and methylerythritol phosphate (MEP; **2**; Scheme 1) and is a key enzyme in the bacterial non-mevalonate pathway to terpenoids.[1] DXR introduces the key branching structure required for the eventual production of isopentenyl diphosphate and dimethylallyl diphosphate by catalysing an apparent α-ketol isomerisation followed by an NADPH-mediated aldehyde reduction.[2] The reaction catalysed by DXR is facilitated by a bound Mn^{2+} ion. Inhibition of the non-mevalonate pathway is lethal to bacteria, and the antibiotic fosmidomycin (**3a**) acts by binding strongly to DXR as a slow tight-binding inhibitor.[3] X-ray crystal structures of DXR from *E. coli*[4,5] and *Zymomonas mobilis*[6] have been solved. Structures of the enzyme, with Mn^{2+} and **3a** bound at the active site, have also been obtained.[7] More recently, structures of *E. coli* DXR in complex with **3a** have been obtained that lack the metal ion.[8]

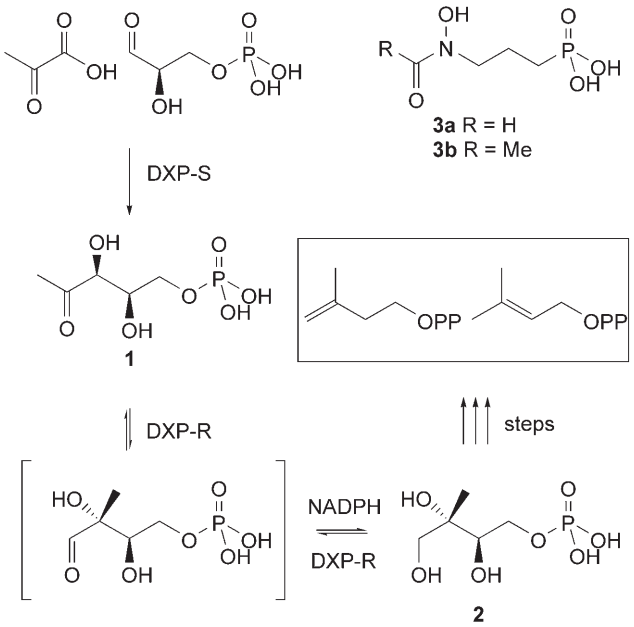

Scheme 1. Non-mevalonate pathway to the terpenoid precursors dimethylallyl diphosphate and isopentenyl diphosphate. DXS, 1-deoxy-D-xylulose-5-phosphate Synthase; DXR, 1-deoxy-xylulose-5-phosphate reductoisomerase (also known as methylerythritol phosphate (MEP) synthase).

There is currently a resurgence in the requirement for new antimicrobial compounds due to the increase in antibiotic resistance. DXR appears to be an attractive target for the development of new inhibitory compounds with antibacterial activity. The recent demonstration that **3a** is effective against the malaria parasite, *Plasmodium*, suggests that DXR inhibitors could also provide a new class of antimalarial compounds.[9] We have already developed a flexible synthesis for **1**[10] and we

[a] *Dr. L. Mercklé, A. de Andrés-Gómez, B. Dick, Dr. R. J. Cox*
School of Chemistry, University of Bristol
Cantock's Close, Clifton, Bristol, BS8 1TS (UK)
Fax: (+44) 117-929-8611
E-mail: r.j.cox@bris.ac.uk

[b] *Dr. C. R. A. Godfrey*
Syngenta, Jealotts's Hill International Research Centre
Jealott's Hill, Bracknell, Berkshire, RG42 6EY (UK)

Supporting information for this article is available on the WWW under http://www.chembiochem.org or from the author.

now report the results of efforts to understand the inhibition of DXR by **3a** and the design and synthesis of new inhibitors.

Results

Several recently published structures of DXR are available. However, the most interesting from the point of view of inhibitor design are those that show bound Mn^{2+} and the inhibitor **3a**.[7] In these structures, it can be observed that the Mn^{2+} ion is held in place by several carboxylates (Asp150, Glu152 and Glu231) and that the metal takes up the expected octahedral geometry. The vacant sites are filled by water molecules in the apo structure. When **3a** is bound, two of the equatorial sites are occupied by the carbonyl oxygen and *N*-hydroxy oxygen atoms of the hydroxamic acid group (Figure 1). Fosmidomycin

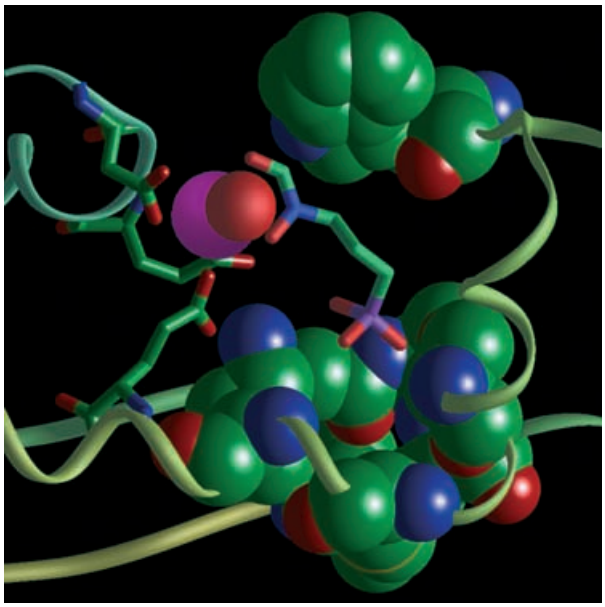

Figure 1. Active site of DXR showing bound **3a.** Mn^{2+} is represented by a purple sphere, with the axial water ligand shown as a red sphere. The Mn^{2+} is also ligated by Asp150, Glu152 and Glu231. The phosphate binding pocket is also shown, as is Trp212 (top) which forms part of the flexible loop. Coordinates were obtained from PDB entry 1ONP.[7]

(**3a**) also possesses a phosphonate which binds to a site defined by Lys228, Gly185, Ser186, Gly187, Ser222, Met225 and Ile250. The top of the active site is defined by Trp212. When both Mn^{2+} and fosmidomycin are bound, a flexible loop that consists of residues 210–215 relocates to cover the active site.[7] It appears likely that **3a** mimics substrate **1**, with the binding such that the phosphonate of **3a** mimics the 5-phosphate of **1**. Meanwhile, the hydroxamic acid of **3a** binds the metal; this perhaps mimics a transition state in the reaction coordinate of **1**. Interestingly the *N*-acetyl analogue of **3a** (FR 900098, **3b**) also strongly inhibits DXR; this suggests that there is sufficient space in the active site to accommodate at least an additional methyl group.[9]

We initially examined the kinetics of the inhibition of DXR by **3a**. We have previously reported the cloning and expression of *E. coli* DXR by using an *N*-terminal hexahistidine tag to aid purification. This enzyme was used to set up assays that

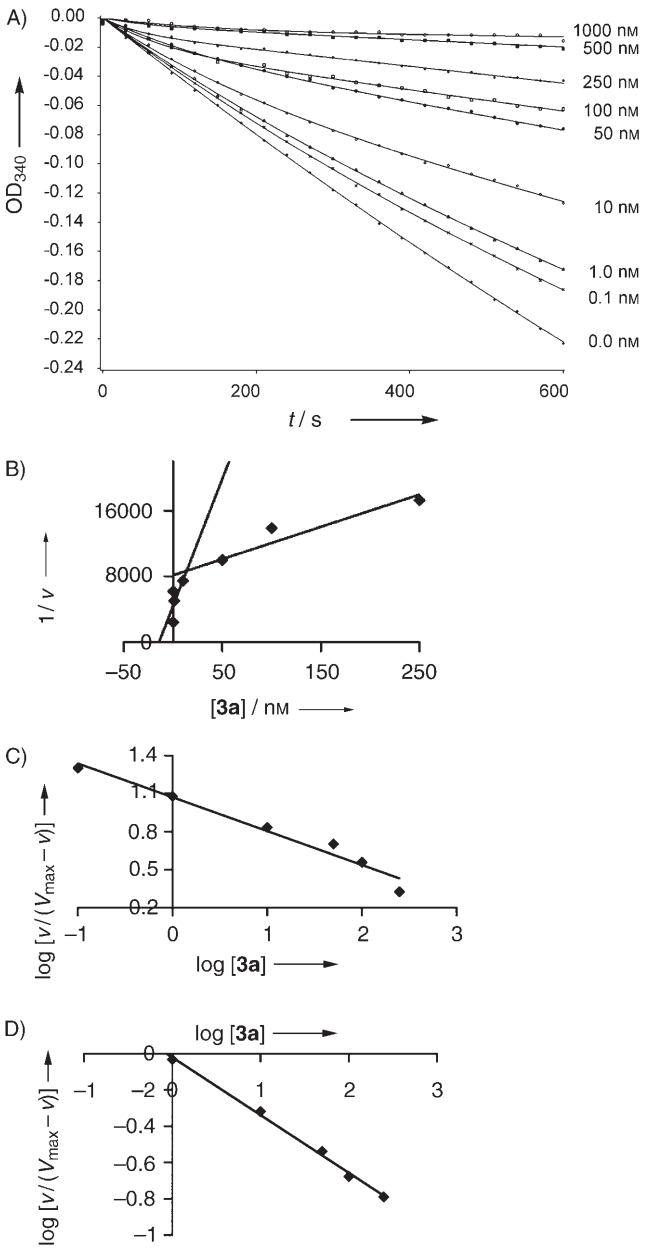

Figure 2. Onset of Inhibition by fosmidomycin **3a** at indicated concentrations. A) Data were collected every 2 s (points shown every 30 s for clarity) and fitted to the integrated rate equations of Morrison and Walsh[11] (curve). B) Reciprocal final equilibrium rate vs. [**3a**] showing biphasic effect. C) Initial rates were extracted and subjected to Hill analysis. D) Equilibrium rates were extracted and subjected to Hill analysis.

were suitable for kinetic analysis in conjunction with synthetic substrate **1**.[10] Assay conditions were optimised to give reproducible rate data. The standard substrate assay consisted of Tris buffer (pH 8.0) that contained Mn^{2+} ions (1.0 mM), NADPH (0.4 mM) and enzyme (1 nM). Addition of substrate **1** (0.1–1 mM) initiated the reaction and NADPH consumption was monitored at 340 nm and 37 °C. Under these conditions the K_M for **1** was 400 μM.

In order to study the inhibition of DXR by **3a** we modified the standard assay conditions to contain less enzyme (0.1 nM); thus the reaction could be monitored over longer time peri-

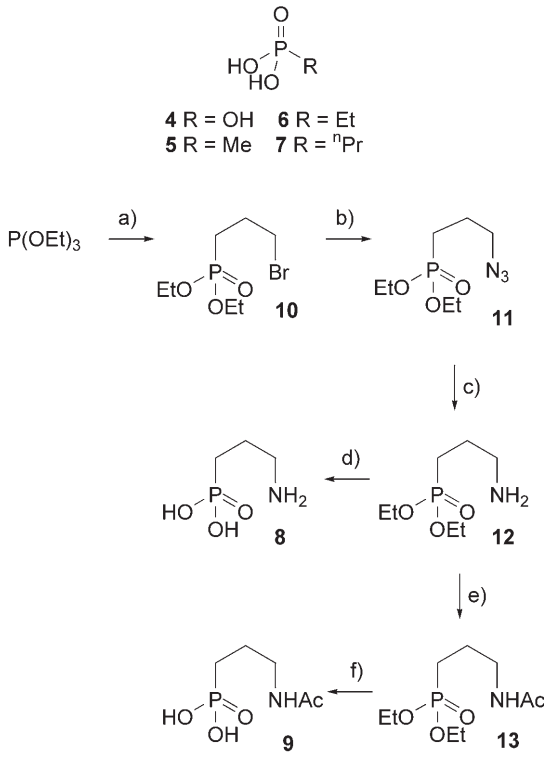

Scheme 2. Analogues of **3a**. a) $Br(CH_2)_3Br$, Δ, 60%; b) NaN_3, EtOH, Δ, 16 h, 51%; c) H_2 (1 atm), Pd/C, EtOH, 78%; d) aq. HCl, Δ, 22 h, 76%; e) Ac_2O, Et_3N, RT, 90%; f) Me_3SiBr, CH_2Cl_2, then aq. KOH, RT, 60%.

ods. We initiated the reaction by adding a mixture of substrate **1** and **3a**. We then followed the progress of the reaction over 1200 s for varying inhibitor concentrations between 1000 and 0.1 nM (Figure 2A). The reactions followed the expected pattern for slow-binding inhibition: initial rapid reaction was followed by a period of increasing inhibition and eventual equilibrium inhibition. In order to determine initial and equilibrium rates of reaction at varying inhibitor concentrations, [I], we fitted the reaction progress curves to the integrated rate equations previously described by Morrison and Walsh.[11] The results of this analysis indicated that in the first few seconds of reaction a rapid equilibrium is established between DXR and **3a**. However, over a period of minutes, a second more tightly bound equilibrium is established. Plots of reciprocal rate as a function of [I] for both initial and equilibrium rates were made (Figure 2B). A curve was obtained, which is indicative of cooperative effects. Hill analysis (i.e., plotting $\log(v/V_{max}-v)$ as a function of log [I],[12] Figure 2C) showed that the initial rapid equilibrium is subject to negative cooperativity ($|h|=0.27$, $K_{0.5}=10.5$ μM). Similar negative cooperativity is observed ($|h|=0.32$, $K_{0.5}=0.9$ nM) at final equilibrium (Figure 2D), but the end inhibition is 10^4-fold tighter.[13]

In order to further probe the slow-binding nature and the observed negative cooperativity of **3a** binding to DXR, we examined the inhibition of DXR by a series of **3a** fragments. A series of phosphate analogues consisting of phosphate itself (**4**), methyl- (**5**), ethyl- (**6**) and propyl- (**7**) phosphonic acids was commercially available. 1-Amino-3-phosphonopropane (**8**) and *N*-acetyl-1-amino-3-phosphonopropane (**9**) were synthesised by single Arbusov reaction of 1,3-dibromopropane to give the monobromide (**10**) (Scheme 2). Displacement of bromide by azide gave **11** and catalytic hydrogenolysis afforded the amine **12**. Acetylation then yielded the amide **13** as a mixture of rotamers. Phosphonate esters **12** and **13** were deprotected by using aqueous acid and base, respectively.

Compounds **4**–**9** were tested as inhibitors in a standard substrate assay in which the concentrations of substrate **1** and inhibitor were varied. All phosphates and phosphonates were found to inhibit the DXR-catalysed reaction (Table 1). Plots of $1/v$ as a function of [I] were curved when phosphate (**4**), methylphosphonate (**5**) and propylphosphonate (**7**) were used as inhibitor. In these cases, Hill analysis indicated *positive* cooperativity (Figure 3) with inhibition constants ($K_{0.5}$) of 40, 32 and 12 mM, respectively. The other compounds showed negligible cooperativity. Ethyl phosphonate appeared to be a competitive inhibitor (K_i 18 mM) while aminopropylphosphonate (**8**) was the most potent inhibitor (K_i 4 mM).

Table 1. Measured inhibition constants.[a]

	K_i	$K_{i(low)}$	$K_{i(high)}$	$\|h\|$	$K_{0.5}$	mode
3a (early)	–	27.2 ± 1.3 nM	244 ± 4 nM	0.27 ± 0.04	10.5 μM	–
3a (late)	–	4.1 ± 0.6 nM	59.0 ± 8.8 nM	0.32 ± 0.03	0.9 nM	–
4	–	250	26.1	2.0 ± 0.5	39.8 ± 3.2	–
5	–	42.5	0.2	2.3 ± 0.16	32.5 ± 2.3	–
6	18.0 ± 4.0	–	–	–	–	C
7	–	8.3	7.0	1.7 ± 0.2	11.9 ± 1.4	–
8	4.0 ± 1.2	–	–	–	–	N/M
9	6.5 ± 0.7	–	–	–	–	N
(±)-**14**	0.75 ± 0.21	–	–	1.2 ± 0.15	2.4 ± 0.3	C
(*S*)-**21**	4.1 ± 1.6	–	–	–	–	N/M
(*S*)-**28**	–	0.9	4.9	0.7 ± 0.20	8.3 ± 2.3	N/U
(*R*)-**21**	–	0.8	11.3	0.5 ± 0.13	4.2 ± 1.0	N/U
(*R*)-**28**	–	1.0	14.0	0.8 ± 0.04	6.4 ± 0.3	N/U

[a] K_i is the inhibition constant for reversible inhibition, $K_{i(low)}$ is calculated for cooperative inhibition at low [I], $K_{i(high)}$ is calculated for cooperative inhibition at high [I], $|h|$ is the Hill coefficient, $K_{0.5}$ is the concentration at which half of the active sites are filled (obtained from Hill analysis) and the mode indicates whether the inhibition was competitive (C), uncompetitive (U), noncompetitive (N) or mixed (M). All *K* values in mM, unless otherwise indicated. Errors are ± 15% unless otherwise indicated. For **3a**, "early" values are for the initial rapid equilibrium, while "late" values are for the final equilibrium (which correspond to K_i^*).

N-acetyl phosphonate (**9**) could not be assayed for inhibition under the standard conditions because interaction with Mn^{2+} in the buffer masked the UV absorbtion of NADPH. However, inhibition was observed in the presence of Mg^{2+}: **9** acted as a noncompetitive inhibitor ($K_i=6.5$ mM) with no apparent cooperative effects.

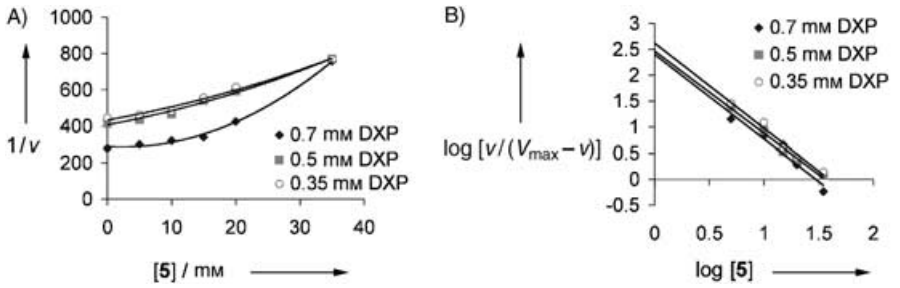

Figure 3. Inhibition by methylphosphonate (**5**) at varying DXP concentrations. A) Plot of $1/v$ as a function of [**5**] showing biphasic inhibition characteristics. Rate (v) units: $AU_{340}\,s^{-1}$. B) Hill analysis (average values: $R^2 = 0.9703$, $|h| = 2.3 \pm 0.16$, $K_{0.5} = 32.5 \pm 2.3$ mM).

Fosmidomycin (**3a**) is a flexible molecule, and it would be expected to show a significant negative entropy change upon binding to DXR. Since Williams et al. have shown that cooperative effects can be related to flexibility and movement of enzyme-bound species,[14] and because it is recognised that rigidification of enzyme inhibitors can increase their potency by ameliorating the entropy loss of binding,[15] we considered simple rigid cyclic analogues of **3a**, such as, (*S*)-**14** (Figure 4) as

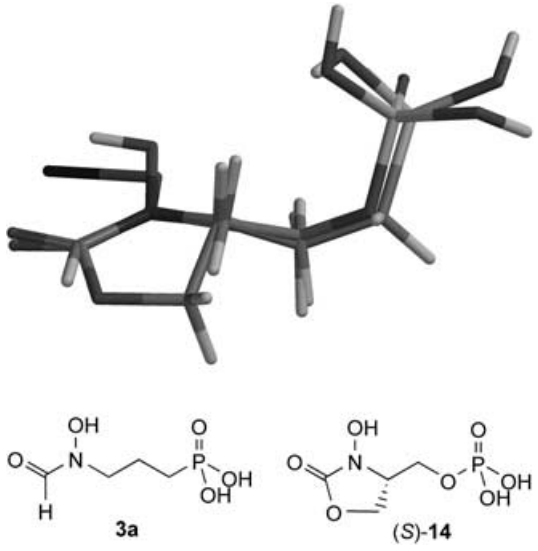

Figure 4. Overlay of **3a** in its bound conformation with (*S*)-*N*-hydroxy-4-(phosphoryloxy)methyloxazolidin-2-one, (*S*)-**14.** The overlay was performed with Spartan (Wavefunction, Inc.) by using a model of the oxazolidinone that was minimised with molecular mechanics calculations. Mn^{2+} is shown bound to the carbonyl of **3a**.

potential potent inhibitors of DXR. We performed simulated-docking experiments with both **3a** and (*S*)-**14**. These studies were not satisfactory, however, because the SYBYL forcefield used by the FLEXX package was not able to correctly place the manganese-binding hydroxamic acid motif of either **3a** or (*S*)-**14** during binding (Figure 5). However, overlay-modelling suggested that (*S*)-**14** can take up a conformation that is almost identical to bound **3a** (Figure 4), and could thus potentially inhibit DXR.

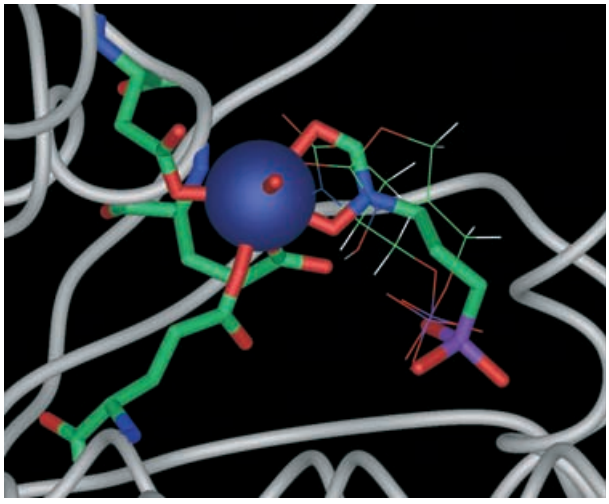

Figure 5. Simulated docking studies of (*S*)-**14.** Experiments were carried out by using the FLEXX package (Tripos Software). The two highest ranked docked structures are shown (wires) and **3a** is shown in its actual bound conformation (sticks).

Synthesis

Initial attempts to obtain (*S*)-**14** began with serine. Thus, L-serine (**15**) was methylated in high yield, and the resulting methyl ester (**16**) was treated with triphosgene to form the cyclic carbamate (**17**) in good yield (Scheme 3).[16] Reduction of **17** with $NaBH_4$ afforded the corresponding primary alcohol (**18**), which was phosphorylated by using the phosphoramidite method. This was followed by *meta*-chloroperbenzoic acid (*m*CPBA) oxidation, to give the dibenzylphosphate ester (*S*)-**19** in moderate yield. D-Serine provided the enantiomeric material (*R*)-**19** by the same procedure.

The regioisomer of **19** was synthesised from L-malic acid (**22**; Scheme 4). Treatment of **22** with trifluoroacetic anhydride in benzyl alcohol selectively afforded the α-benzyl ester **23** in good yield. Cyclic carbamate formation was achieved by using diphenylphosphoryl azide to give **24**.[17] Once again, $NaBH_4$ reduction and phosphorylation gave the required cyclic carbamate, (*S*)-**26**, which was protected as the bisbenzyl ester. D-Malic acid gave the enantiomer (*R*)-**26** as expected. At this stage we attempted *N*-oxidation of **19** and **26**. However, despite literature reports of the successful use of trifluoromethyldioxirane[18] and Mo reagents[19] in similar reactions, we did not observe *N*-oxidation of either **19** or **26**.

An alternative strategy was then followed to obtain the *N*-hydroxycarbamates (Scheme 5). Clearly late *N*-oxidation was not possible, so we decided to use an intact N–O linkage from the beginning of the synthesis. Thus dihydroxyacetone (**29**) was treated with *O*-benzylhydroxylamine in methanol to afford

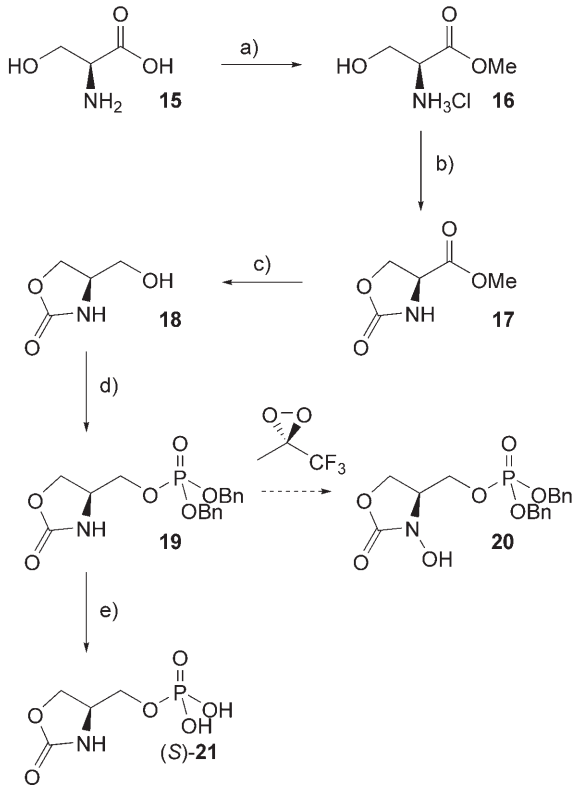

Scheme 3. Synthesis of 4-substituted oxazolidin-2-ones. a) MeOH, HCl, Δ, quant.; b) $(CCl_3)_2CO$, Et_3N, CH_2Cl_2, 0 °C, 79%; c) $NaBH_4$, EtOH, 0 °C, 82%; d) $iPr_2NP(OBn)_2$, $PhNH_2Me^+TFA^-$, CH_2Cl_2, then *m*CPBA, 52%; e) H_2 (1 atm), Pd/C, EtOH, 99%.

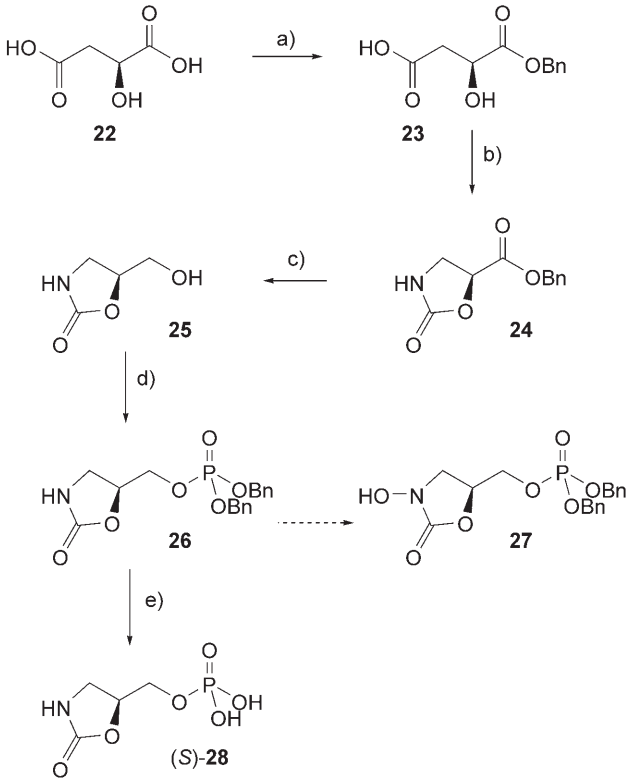

Scheme 4. Synthesis of 5-substituted oxazolidin-2-ones. a) $(CF_3CO)_2O$ then BnOH, 77%; b) Et_3N, $(PhO)_2P(O)N_3$, toluene, Δ, 77%; c) $NaBH_4$, EtOH, 0 °C, 87%; d) $iPr_2NP(OBn)_2$, $PhNH_2Me^+TFA^-$, CH_2Cl_2, then *m*CPBA, 29%; e) H_2 (1 atm), Pd/C, EtOH, quant.

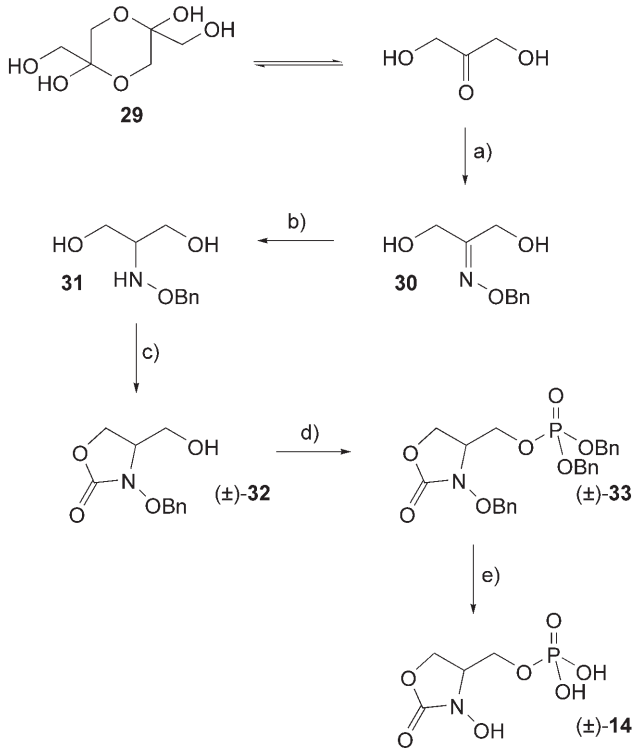

Scheme 5. Synthesis of *N*-hydroxy 4-substituted oxazolidin-2-one, (±)-**14**. a) H_2O, $BnONH_3Cl$, quant; b) $NaBH_3CN$, MeOH, TFA, 84%; c) $(CCl_3)_2CO$, *N*,*N*′-diisopropylethylamine (DIPEA), CH_2Cl_2, 0 °C, 47%; d) $iPr_2NP(OBn)_2$, $PhNH_2Me^+TFA^-$, CH_2Cl_2, then *m*CPBA, 62%; e) H_2 (1 atm), Pd/C, MeOH, 51%.

the corresponding oxime **30** in excellent yield. Cyanoborohydride-mediated reduction then gave the 2-benzyloxyaminopropane diol **31** in good yield. Treatment of achiral **31** with triphosgene then afforded carbamate (±)-**32** which underwent phosphorylation under standard conditions to afford the desired (albeit racemic) protected *N*-hydroxycarbamate **33**.

Deprotection of the benzyl-protected carbamates **19** and **26** and *N*-hydroxycarbamate **33** was achieved by hydrogenolysis over 10% Pd on carbon catalyst, which give **21**, **28** and **14**, respectively. In the case of the *N*-hydroxy compound (±)-**14**, mass spectrometric analysis confirmed the intact N–O linkage.

Compounds (*S*)-**21**, (*R*)-**21**, (*S*)-**28** and (*R*)-**28** and the racemic *N*-hydroxycarbamate (**14**) were examined as inhibitors of DXR. Inhibition assays were performed by measuring the rate of reaction (*v*) at varying substrate [S] and inhibitor [I] concentrations. Carbamates (*S*)-**21**, (*R*)-**21**, (*S*)-**28** and (*R*)-**28** were found to inhibit DXR (Figure 6A, Table 1)—albeit rather weak—in the high-μM to low-mM range. However, efforts to characterise the mode of inhibition by plotting $1/v$ as a function of either [I] or 1/[S] resulted in curved plots for (*R*)-**21**, (*S*)-**28** and (*R*)-**28** (Figure 6B). A typical dataset (for compound (*R*)-**21** at fixed [DXP] of 0.5 mM; Figure 6B) showed two phases of inhibition—at low [I], an apparent K_i of 0.8 mM was measured. However, by increasing inhibitor concentration a different K_i value of 11.3 mM was obtained. Hill analysis clearly showed a linear relationship indicating negative cooperativity (i.e., Hill coefficient, $|h| < 1$) for (*R*)-**21**, (*S*)-**28** and (*R*)-**28** (Figure 6C, Table 1).

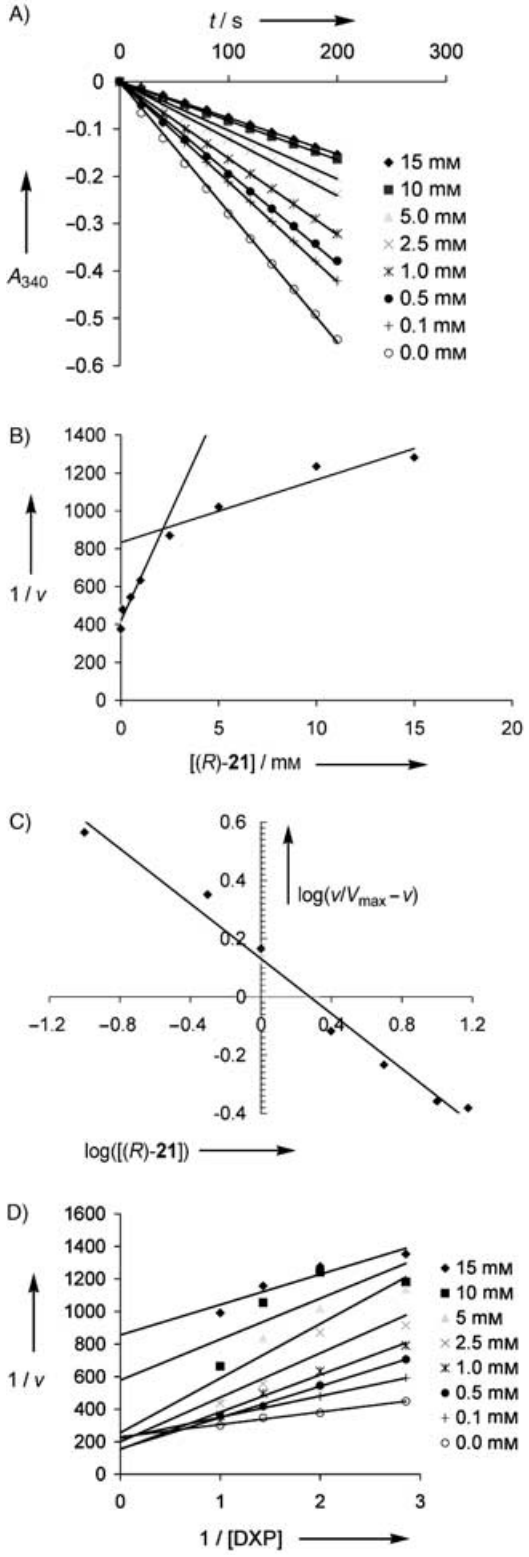

Figure 6. Inhibition of DXR by carbamate, (*R*)-**21**. A) Inhibition by (*R*)-**21** showing reducing rate of NADPH consumption with increasing (*R*)-**21** concentration. B) Replot of 1/*v* as a function of [(*R*)-**21**] showing biphasic inhibition characteristics. Rate (*v*) units: $AU_{340}{\cdot}s^{-1}$.C) Hill analysis ($R^2 = 0.981$, $|h| = 0.5$, $K_{0.5} = 4.2$ mM). Note that the Hill coefficient is *negative* because as the inhibitor concentration increases, the reaction rate decreases. D) Attempt to determine the mode of inhibition by using Lineweaver–Burk analysis at varying inhibitor (*R*)-**21** concentrations.

Inhibitor (*S*)-**21** showed no obvious cooperative behaviour, only noncompetitive/mixed inhibition. Assays designed to detect time-dependent inhibition did not indicate any covalent or slow-binding behaviour for any of the cyclic carbamates.

In order to analyse the inhibition further, plots of 1/*v* as a function of 1/[S] at varying inhibitor concentrations were made for (*R*)-**21**, (*S*)-**28** and (*R*)-**28** (Figure 6D). Because the inhibition varied with inhibitor concentration due to the negative cooperativity, we treated the data in two sets—one at lower [I], the other at higher [I]. The resulting plots indicated that at lower [I] the inhibition could be classified as noncompetitive, while at higher [I] the pattern changed to uncompetitive.

We expected the racemic *N*-hydroxycarbamate (±)-**14** to show inhibition that was comparable with that of **3a** ($K_{0.5}$ 0.9 nM in our assays, vide supra). However kinetic analysis showed simple competitive inhibition with a K_i of 0.75 mM. Data analysis indicated no cooperative or time-dependent behaviour.

Discussion

Previous investigations of DXR have focussed on two main areas: crystallographic structure solutions, and biochemical and kinetic analysis of substrates and substrate analogues. Two inhibitors of DXR, **3a** and **3b**, have also been investigated, but very few systematic attempts to design and synthesise new inhibitors, beyond simple substrate analogues, have been reported.[20,21] The structural and biochemical results reported to date show that DXR is a homodimer, with one active site per subunit, and support a mechanism in which **1** binds before NADPH. It is suggested that a flexible loop consisting of residues 210–215 becomes more ordered upon substrate binding.[5] The first reaction catalysed is an apparent concerted α-ketol rearrangement or stepwise fragmentation-reassembly mechanism. No conclusive evidence that rules out one of these pathways has been found, but it is certain that the intermediate(s) remain tightly bound to DXR prior to NADPH mediated reduction. After reduction it is suggested that $NADP^+$ leaves before the product MEP (**2**).

DXR requires activation by a divalent metal ion; Co^{2+}, Mn^{2+} and Mg^{2+} have been shown to activate the enzyme, albeit with varying kinetic parameters.[22] It has also been reported that the kinetic parameters for substrate binding vary with the metal, and that the DXR catalysed reactions can actually slow down with increasing NADPH concentration.[2] For these reasons we studied inhibition of DXR at fixed metal (Mn^{2+}) and NADPH concentrations which were chosen to reflect conditions described in the literature. These concentrations also gave reproducible, linear, NADPH-consumption curves in our assays (e.g., Figure 6A). Under these conditions, with synthetic **1**, K_M was 400 μM, which is similar to the value of 250 μM measured by Seto and co-workers,[23] but somewhat higher than the 115 μM measured by Poulter et al.[3] However, differences in K_M are to be expected as the K_M for any given substrate varies with the concentration of other substrates. Additionally, differences might be due to the fact that the DXR used in our work and by Seto et al. has a hexahistidine *N*-terminal exten-

sion in contrast to the native DXR used by Poulter and coworkers.

Hill analysis of substrate data (not shown) gave a Hill coefficient of $|h| = 1.0$; this indicates no cooperativity during substrate processing. However, when we examined inhibition by **3a**, we observed that the expected slow-binding inhibition displayed significant negative cooperativity—that is, as inhibitor concentration increases, the apparent K_i increases. The measured Hill constants for both the initial binding process and final equilibrium were similar. Because the measured K_i varies with inhibitor concentration (or, as shown here, the range of concentrations over which K_i is calculated), comparisons of measured K_i values with previous studies are difficult. We calculated two K_i values: $K_{i(low)}$ at relatively low **3a** concentrations (below 50 nM) and $K_{i(high)}$ at relatively high **3a** concentrations (above 50 nM). Thus four K_i values can be obtained for inhibition of DXR by **3a** (Table 1). Two other groups have measured initial (K_i) and final (K_i^*) equilibrium for inhibition of DXR by **3a**. However, they have not examined inhibition over the wide range of **3a** concentrations that is required to observe cooperativity. Poulter et al. obtained values for K_i and K_i^* of 215 nM and 21 nM, respectively,[3] while Rohmer et al. have reported K_i to be 40 nM and K_i^* to be 10 nM.[21] Both sets of data were obtained at **3a** concentrations above 50 nM.

In order to investigate this phenomenon in more detail, we examined inhibition by phosphate, methyl-, ethyl-, propyl-, 3-aminopropyl- and *N*-acetyl-3-(aminopropyl)phosphonic acids, each of which is a fragment of **3a** (or its *N*-acetyl analogue, **3b**). Phosphate itself inhibited weakly, but methyl-, ethyl- and propylphosphonic acids showed increasingly stronger inhibition. Phosphate, methylphosphonate and propylphosphonate displayed *positive cooperativity* (i.e., the apparent K_i decreases as inhibitor concentration increases). However, negligible cooperativity of inhibition was observed for ethyl-, aminopropyl- and *N*-acetylaminopropylphosphonates. When the compounds resemble **3a** more closely, the K_i values of improve marginally; although the most potent (**8**) is still less potent than **3a** at equilibrium by a factor of 10^6. It is noteworthy, however, that initial binding of **3a** at 10.5 μM is just 10^2-fold better than **8** and **9**.

Carbamates (*S*)-**21**, (*S*)-**28**, (*R*)-**21** and (*R*)-**28** also inhibited DXR in the mM range. (*R*)-**21**, (*S*)-**28** and (*R*)-**28** showed negative cooperativity similar to **3a**, whereas (*S*)-**21** showed negligible cooperativity. None of the carbamates showed time-dependent inhibition.

It is not possible to distinguish true negative cooperativity, which involves "communication" between identical active sites on separate subunits, from binding at two separate sites with differing potencies, because they are kinetically indistinguishable.[12] However, positive cooperativity *must* arise from binding at two identical sites—that is, when phosphate and methylphosphonate bind at one active site on one subunit of DXR, there must be "communication" to the second subunit. This then results in enhanced binding of the second equivalent of inhibitor. The existence of this communication makes it likely that the negative cooperativity observed in the case of **3a** and cyclic carbamates is also due to communication between active sites on the two subunits of the DXR dimer.

Crystal structure data for DXR with bound inhibitors and with vacant active sites indicate that a flexible loop consisting of residues 210–215 undergoes a large conformational change when inhibitors bind (Figure 7). Recent crystal structure data from Yajima and Oldfield et al. show DXR binding to two bisphosphonate compounds (with low-μM inhibition constants).[24] However, the phosphonate moieties of these compounds do not bind in the phosphate binding site that is utilised by **3a**; instead they bind to the metal ion. Another difference is that the loop region forms a different conformation when it is located over the bisphosphonate inhibitors rather than over **3a**.

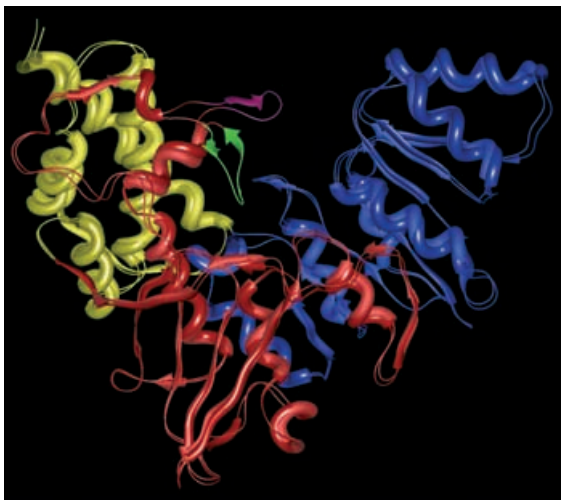

Figure 7. Overlay of DXR monomer crystal structures showing the extent of flexible loop movement upon **3a** binding. The apo structure coordinates (shiny metal, purple loop) were obtained from pdb 1K5H, the holo structure coordinates (plastic, green loop) were obtained from pdb 1ONP. The overlay was performed by using the programme iMol. The structure shows the NADPH binding domain (blue), the catalytic and dimerisation domain (red) and the "structural" domain (yellow).

Loop movement could explain both the observed cooperativity in inhibition and the slow-binding inhibition by **3a**. Our results are consistent with a mechanism in which inhibitors can initially bind at either, or both, of the metal ion and phosphate binding sites in one of the subunits of the dimeric DXR. Binding is accompanied by a loop movement that could then transmit a conformational change to the active site in the second subunit of the DXR dimer. This initial binding has K_i values in the μM to mM range. In the case of **3a** (which binds at both phosphate and metal ion sites) a second slower process occurs which tightens the binding by a factor of approximately 10^4. We interpret this as a further loop movement, which perhaps brings Trp212 into closer proximity with the hydrophobic portion of **3a**. Our results support a mechanism in which initial binding of **3a** to DXR is subject to cooperativity, but the subsequent slow approach to tight-binding does not change the initial cooperativity. Transmission of conformational

changes between enzyme subunits has been observed previously. For example, Stroud et al. have shown that the enzyme thymidylate synthase undergoes a conformational change in one subunit upon cofactor binding; this then prevents cofactor binding in the other subunit.[25]

Very recently further crystallographic evidence has emerged that shows how the structure of DXR sequentially closes as each ligand binds and eventually forms a tightly bound closed complex. The process appears to be driven by a reduction in exposed hydrophobic surfaces.[8] Our kinetic evidence supports this interpretation and lends weight to the crystallographic evidence for a two-step inhibition process.[8]

None of the other inhibitors tested here showed time-dependent inhibition of DXR; this suggests that they are not able to take up a conformation that is capable of inducing full-loop closure. This is supported by structures available for binding by bisphosphonates which show the loop in an alternative position.[24] Reports to date have not discussed the kinetics of inhibition of these compounds.

Explanations for the observed positive or negative cooperativity are more difficult to formulate—it might be that different loop movements induced by various inhibitors are transmitted between subunits in distinct ways. For example, the only compounds that showed positive cooperative inhibition were the relatively small phosphate, methyl- and propylphosphonates—these might bind more strongly at the Mn^{2+} site, while all the other (larger) compounds might bind preferentially at the phosphate binding site.

Surprisingly the *N*-hydroxy cyclic carbamate (±)-**14** which is a close structural analogue of **3a** showed neither cooperative nor time dependent inhibition of DXR. It was at least 10^6-fold less potent than **3a** itself, despite the fact that modelling and docking studies suggested it should be able to bind to DXR. This is probably due to prevention of full loop-movement caused by improper binding at the metal. This illustrates two significant problems with simulated-docking strategies with DXR. The first is that standard force-field implementations are inadequate for simulating metal binding, and secondly—and more seriously—the large changes in flexible loop conformation which accompany inhibitor binding cannot be simulated. It thus appears unlikely that our efforts to design potent new inhibitors of DXR will be aided by docking studies, and we are presently investigating crystallographic approaches to understanding the interaction of DXR's flexible loop with small molecules.

Experimental Section

Synthetic details for compounds **8**, **9**, **11**–**14**, **19**, **21**, **26**, **28** and **30**–**33** are contained in the Supporting Information.

Enzyme assays: Buffers and stock solutions were made with deionised water and ACS grade reagents. The assay was monitored spectrophotometrically through the consumption of β-NADPH. It was observed at 340 nm in a Pharmacia-LKB Ultrospec III UV spectrophotometer that was equipped with a heated-water jacket cuvette. The pH was measured at RT with a KCl electrode and PW9418 analogue pH meter (Philips). All TRIS buffers were adjusted to pH 8.0 at 37 °C. In order to keep a constant temperature throughout the assay, the buffer solution was held in a 37 °C water bath; the UV cell jacket was also at 37 °C. The other stock solutions were kept in ice prior to addition.

Standard assay: The apparatus was calibrated to 0.00 OD_{340} units with buffer solution (0.1 M Tris, 0.1 mM DTT, 1 mM Mn^{2+}). Buffer solution (980 μL, 0.1 M Tris, 0.1 mM DTT, 1 mM Mn^{2+} and 0.4 mM β-NADPH) and then DXR (10 μL, 100 nM) were introduced sequentially into a 1000 μL Quartz UV cuvette. The cuvette was mixed by inversion three times, introduced into the UV spectrophotometer, which was set at 340 nm, and data collection was started. Data points were collected every 2 s. After 4 s, a stock solution of **1** (100 mM) in Tris buffer (10 μL, 100 mM) was added. The mixture was inverted three times, and the enzymatic reaction was monitored over 330 s. The data obtained was then processed by using Microsoft Excel.

Inhibitory assay (example at 1 mM inhibitor): After calibration (see standard assay), buffer solution (970 μL, 0.1 M Tris, 0.1 mM DTT, 1 mM Mn^{2+}, 0.4 mM β-NADPH), DXR (10 μL, 100 nM) and inhibitor stock solution (0.1 M) in Tris buffer (10 μL, 100 mM) were introduced, in order, into a 1000 μL Quartz UV cuvette. The cuvette was inverted three times, placed into the UV spectrophotometer which was set at 340 nm and data collection initiated. After 4 s, a stock solution of **1** (100 mM) in Tris buffer (10 μL, 100 mM) was added. The mixture was mixed by inversion three times and the enzymatic reaction monitored over 330 s. The data obtained was then processed by using Microsoft Excel. Inhibitor assays contained inhibitor at concentrations of 0.1–15 mM (cyclic analogues) and 5–35 mM (phosphonic acid derivates).

Fosmidomycin (3a) slow-binding assay (example at 100 nM fosmidomycin): After calibration (see standard assay), buffer solution (970 μL, 0.1 M Tris, 0.1 mM DTT, 1 mM Mn^{2+}, 0.4 mM β-NADPH), **3a** stock solution in Tris buffer (10 μL, 10 μM) and **1** stock solution (100 mM) in Tris buffer (10 μL, 100 mM) were introduced, in order, into a 1000 μL Quartz UV cuvette. The cuvette was mixed by inversion three times, placed in the UV spectrophotometer, which was set at 340 nm, and data collection was initiated. After 4 s, the enzymatic reaction was started by the addition of DXR (10 μL, 10 nM). The mixture was quickly inverted three times, and the enzymatic reaction was monitored over 20 min. The data obtained was fitted directly to the integrated rate equation of Morrison and Walsh[11] by using MacCurveFit.[26] Inhibitor assays contained inhibitor at concentrations of 0.1–1000 nM.

Acknowledgements

A.D.A.G. thanks Syngenta for the provision CASE funding and the School of Chemistry, University of Bristol, for a scholarship. Syngenta are also thanked for the provision of fosmidomycin. L.M. was funded by the BBSRC (7/B17965).

Keywords: antibiotics · enzymes · fosmidomycin · inhibitors · simulated docking

[1] A. Argyrou, J. S. Blanchard, *Biochemistry* **2004**, *43*, 4375 – 4384.
[2] J.-F. Hoeffler, D. Tritsch, C. Grosdemange-Billiard, M. Rohmer, *Eur. J. Biochem.* **2002**, *269*, 4446 – 4457.
[3] A. T. Koppisch, D. T. Fox, B. S. J. Blagg, C. D. Poulter, *Biochemistry* **2002**, *41*, 236 – 243.

[4] K. Reuter, S. Sanderbrand, H. Jomaa, J. Wiesner, I. Steinbrecher, E. Beck, M. Hintz, G. Klebe, M. T. Stubbs, *J. Biol. Chem.* **2002**, *277*, 5378 – 5384.
[5] S. Yajima, T. Nonaka, T. Kuzuyama, H. Seto, K. Ohsawa, *J. Biochem.* **2002**, *131*, 313 – 317.
[6] S. Ricagno, S. Grolle, S. Bringer-Meyer, H. Sahm, Y. Lindqvist, G. Schneider, *Biochim. Biophys. Acta* **2004**, *1698*, 37 – 44.
[7] S. Steinbacher, J. Kaiser, W. Eisenreich, R. Huber, A. Bacher, F. Rohdich, *J. Biol. Chem.* **2003**, *278*, 18401 – 18407.
[8] A. Mac Sweeney, R. Lange, R. P. M. Fernandes, H. Schulz, G. E. Dale, A. Douangamath, P. J. Proteau, C. Oefner, *J. Mol. Biol.* **2005**, *345*, 115 – 127.
[9] H. Jomaa, J. Wiesner, S. Sanderbrand, B. Altincicek, C. Weidemeyer, M. Hintz, I. Turbachova, M. Eberl, J. Zeidler, H. K. Lichtenthaler, D. Soldati, E. Beck *Science* **1999**, *285*, 1573 – 1576.
[10] R. J. Cox, A. de Andres-Gomez, C. R. A. Godfrey, *Org. Biomol. Chem.* **2003**, *1*, 3173 – 3177.
[11] J. F. Morrison, C. T. Walsh, *Adv. Enzymol. Relat. Areas Mol. Biol.* **1988**, *61*, 201 – 301.
[12] A. Fersht, *Enzyme Structure and Mechanism*, 2nd ed., Freeman, New York, **1985**, pp 263 – 292; A. Cornish-Bowden, *Fundamentals of Enzyme Kinetics*, 2nd ed., Portland, London, **1995**, pp 203 – 236.
[13] In all cases discussed here the sign of h is negative, because as the inhibitor concentration increases, the rate of reaction decreases. However, the sense of cooperativity is indicated by the magnitude of h—when $|h| > 1.0$ the effect is positive and when $|h| < 1.0$ the effect is negative.
[14] D. H. Williams, C. T. Calderone, D. P. O'Brien, R. Zerella, *Chem. Commun.* **2002**, 1266 – 1267.
[15] A. R. Khan, J. C. Parrish, M. E. Fraser, W. W. Smith, P. A. Bartlett, M. N. G. James, *Biochemistry* **1998**, *37*, 16839 – 16845.
[16] M. P. Sibi, D. Rutherford, P. A. Renhowe, B. Q. Li, *J. Am. Chem. Soc.* **1999**, *121*, 7509 – 7516.
[17] K. Danielmeier, E. Steckhan, *Tetrahedron: Asymmetry* **1995**, *6*, 1181 – 1190.
[18] A. Detomaso, R. Curci, *Tetrahedron Lett.* **2001**, *42*, 755 – 758.
[19] S. A. Matlin, P. G. Sammes, R. M. Upton, *J. Chem. Soc. Perkin Trans. 1* **1979**, 2481 – 2486.
[20] M. Courtois, Z. Mincheva, F. Andreu, M. Andreu, M.-C. Viaud-Massuard, *J. Enzyme Inhib. Med. Chem.* **2004**, *19*, 559 – 565.
[21] L. Kunz, D. Tritsch, C. Grosdemange-Billiard, A. Hemmerlin, A. Willem, T. J. Bach, M. Rohmer, *Biochem. J.* **2005**, *386*, 127 – 135.
[22] S. Takahashi, T. Kuzuyama, H. Watanabe, H. Seto, *Proc. Natl. Acad. Sci. USA* **1998**, *95*, 9879 – 9884.
[23] T. Kuzuyama, S. Takahashi, M. Takagi, H. Seto, *J. Biol. Chem.* **2000**, *275*, 19928 – 19932.
[24] S. Yajima, K. Hara, J. M. Sanders, F. Yin, K. Ohsawa, J Wiesner, H. Jomaa, E. Oldfield, *J. Am. Chem. Soc.* **2004**, *126*, 10824 – 10825.
[25] A. C. Anderson, R. H. O'Neil, W. L. DeLano, R. M. Stroud, *Biochemistry* **1999**, *38*, 13829 – 13836.
[26] MacCurveFit (also available for Windows) is shareware available from http://www.krs.com.au/mcf.html

Received: February 10, 2005
Published online on August 23, 2005

